JOURNAL OF GUIDANCE, CONTROL, AND DYNAMICS
Vol. 33, No. 6, November–December 2010

Robust Flight Control Using Incremental Nonlinear Dynamic Inversion and Angular Acceleration Prediction

S. Sieberling,* Q. P. Chu,† and J. A. Mulder‡
Delft University of Technology, 2629 HS Delft, The Netherlands

DOI: 10.2514/1.49978

This paper presents a flight control strategy based on nonlinear dynamic inversion. The approach presented, called incremental nonlinear dynamic inversion, uses properties of general mechanical systems and nonlinear dynamic inversion by feeding back angular accelerations. Theoretically, feedback of angular accelerations eliminates sensitivity to model mismatch, greatly increasing the robust performance of the system compared with conventional nonlinear dynamic inversion. However, angular accelerations are not readily available. Furthermore, it is shown that angular acceleration feedback is sensitive to sensor measurement time delays. Therefore, a linear predictive filter is proposed that predicts the angular accelerations, solving the time delay and angular acceleration availability problem. The predictive filter uses only references and measurements of angular rates. Hence, the proposed control method makes incremental nonlinear dynamic inversion practically available using conventional inertial measurement units.

I. Introduction

FLYING scale models are considered as an additional tool in aircraft design more often and simple unmanned aerial vehicles (UAVs) are used for a growing number of applications such as surveillance and monitoring. One of the objectives in the design of these UAVs is almost always to be low cost. It is often also mandatory to fly automated or at least have sufficient stability augmentation. Unfortunately using current approaches for control system design these objectives are often conflicting. A robust generic flight control system that can easily be implemented to a new type of aircraft using a primitive aerodynamic model can significantly reduce the consumption of resources for flight control system design. This paper presents a solution for such an easily adaptable robust flight control system.

Currently, control techniques exist that are generic in nature, including nonlinear dynamic inversion (NDI) [1]. For flight control purposes, NDI uses an aerodynamic model to linearize the dynamics of an aircraft. The resulting linear system is in principle the same for every aircraft, given that the aerodynamic model is correct. NDI, however, suffers from the major drawback that performance is lost and unstable situations can occur in case of model mismatch.

Several successful attempts have been made to identify and eliminate the flaws of NDI with respect to robustness. Many of the attempts have focused on combining NDI with robust control techniques using μ analysis and H_∞ synthesis, such as in [2–4]. In these references a control law was found with significant benefits over regular NDI. No or little gain scheduling was required and statements concerning the robustness could be made. In many of the publications, however, not all uncertainties are taken into account or they are covered by lumped uncertainties hence introducing conservatism.

The obvious alternative solution to make the controller less sensitive to model mismatch is to make the controller less depending on the model. The present paper presents a method that is not conservative, but still incorporates all uncertainties, by feeding back angular accelerations. This concept is previously described by [5,6]. The control systems showed good performance when subjected to aerodynamic model mismatch. However, the robustness properties of angular acceleration feedback are not explicitly described by the authors. Also, [5,6] assume that the angular accelerations are readily available from measurements.

In [6] the concept of feeding back angular accelerations is derived by first rewriting the rotational dynamic equations of motion into an incremental form and then applying regular NDI, resulting in incremental nonlinear dynamic inversion (INDI). It should be noted that INDI has been referred to by [5] as simplified dynamic inversion. However the authors of the present paper find that the designation incremental nonlinear dynamic inversion better describes the design methodology of the control laws. Rewriting the equations of motion allows for an explicit description of the influence of the uncertainties on the closed-loop system as is demonstrated in this paper. In the present paper the insensitivity to aerodynamic model mismatch, center of gravity mismatch and inertia mismatch are shown, at the cost of sensitivity to sensor measurement delays and the use of measurements that are not readily available.

The origin of measurement sensitivity is discussed and a solution to the problem is presented in the form of a predictive filter for the angular accelerations. The filter is based on only the angular rates and their reference values, using simple polynomial prediction. Which is possible only because of the unique properties of INDI. It is shown that this solves the problems related to sensor measurement delays without significantly degrading the robust performance increases obtained from INDI. Furthermore it is a solution to the practical availability problem of angular accelerations.

The paper is structured as follows: Sec. II discusses the model for which the controller is designed. Section III briefly reviews regular NDI and Sec. IV introduces the novel concept of INDI. Section V reformulates the equations of motion into a form including uncertainties and discusses the influence of these uncertainties on NDI and INDI. Section VI discusses the influence of measurement delays and presents the suggested predictive filter. Section VII briefly discusses outer loop control in the form of sideslip control. In Sec. VIII the results are presented, followed by a discussion, Sec. IX, and conclusions, Sec. X.

II. Model

The control strategy is tested in simulations of a UAV having a T tail and engines attached to the rear end of the fuselage. The engines generate thrust along the aircraft body X axis. The UAV contains

Received 3 April 2010; revision received 17 June 2010; accepted for publication 18 June 2010.

*Researcher, Control and Simulation Division, Faculty of Aerospace Engineering, Kluyverweg 1; s.sieberling@gmail.com.

†Associate Professor, Control and Simulation Division, Faculty of Aerospace Engineering, Kluyverweg 1; q.p.chu@tudelft.nl. Member AIAA.

‡Professor, Control and Simulation Division, Faculty of Aerospace Engineering, Kluyverweg 1; j.a.mulder@tudelft.nl. Member AIAA.

conventional control surfaces, hence an elevator, ailerons and a rudder. The aircraft under consideration has a span of 4.16 m, a reference wing surface area of 1.82 m^2 and a mean aerodynamic chord of 0.48 m. The motion of the aircraft is described by Eqs. (1–4)

$$\begin{bmatrix} \dot{u} \\ \dot{v} \\ \dot{w} \end{bmatrix} = g \begin{bmatrix} -\sin\theta \\ \sin\phi\cos\theta \\ \cos\phi\cos\theta \end{bmatrix} + \frac{1}{m} \begin{bmatrix} \frac{1}{2}\rho V^2 S C_X + T \\ \frac{1}{2}\rho V^2 S C_Y \\ \frac{1}{2}\rho V^2 S C_Z \end{bmatrix} - \begin{bmatrix} qw - rv \\ ru - pw \\ pv - qu \end{bmatrix} \tag{1}$$

$$\begin{bmatrix} \dot{x}_0 \\ \dot{y}_0 \\ \dot{z}_0 \end{bmatrix} = \begin{bmatrix} \cos\psi\cos\theta & -\sin\psi\cos\phi + \cos\psi\sin\theta\sin\phi & \sin\psi\sin\phi + \cos\psi\sin\theta\cos\phi \\ \sin\psi\cos\theta & \cos\psi\cos\phi + \sin\psi\sin\theta\sin\phi & -\cos\psi\sin\phi + \sin\psi\sin\theta\cos\phi \\ -\sin\theta & \cos\theta\sin\phi & \cos\theta\cos\phi \end{bmatrix} \begin{bmatrix} u \\ v \\ w \end{bmatrix} \tag{2}$$

$$\begin{bmatrix} \dot{p} \\ \dot{q} \\ \dot{r} \end{bmatrix} = \bar{\mathbf{J}}^{-1} \left\{ \begin{bmatrix} \frac{1}{2}\rho V^2 S b C_l \\ \frac{1}{2}\rho V^2 S \bar{c} C_m \\ \frac{1}{2}\rho V^2 S b C_n \end{bmatrix} - \begin{bmatrix} p \\ q \\ r \end{bmatrix} \times \left(\bar{\mathbf{J}} \begin{bmatrix} p \\ q \\ r \end{bmatrix} \right) \right\} \tag{3}$$

$$\begin{bmatrix} \dot{\phi} \\ \dot{\theta} \\ \dot{\psi} \end{bmatrix} = \begin{bmatrix} 1 & \sin\phi\tan\theta & \cos\phi\tan\theta \\ 0 & \cos\phi & -\sin\phi \\ 0 & \frac{\sin\phi}{\cos\theta} & \frac{\cos\phi}{\cos\theta} \end{bmatrix} \begin{bmatrix} p \\ q \\ r \end{bmatrix} \tag{4}$$

With the body fixed velocity components $[\,u \quad v \quad w\,]^T$, the body fixed rotational rates $\boldsymbol{\omega} = [\,p \quad q \quad r\,]^T$, the attitude $[\,\phi \quad \theta \quad \psi\,]^T$, the position $[\,x_0 \quad y_0 \quad z_0\,]^T$, the force coefficients $[\,C_X \quad C_Y \quad C_Z\,]^T$ and moment coefficients $\mathbf{C}_M = [\,C_l \quad C_m \quad C_n\,]^T$. $\bar{\mathbf{J}}$ is the moment of inertia matrix, g the gravitational acceleration and m the mass, S the wing surface area, V the airspeed, ρ the air density, b the wing span and $\bar{c}$ the mean aerodynamic chord. The moment and force coefficients are given by a general aerodynamic model, Eqs. (5) and (6), described by, respectively, symmetric and asymmetric control and stability derivatives

$$C_i = C_i\left(\alpha, \frac{\dot{\alpha}\,\bar{c}}{V}, \frac{q\bar{c}}{V}, \delta_e, M\right) \tag{5}$$

$$C_j = C_j\left(\alpha, \beta, \frac{\dot{\beta} b}{2V}, \frac{pb}{2V}, \frac{rb}{2V}, \delta_a, \delta_r, M\right) \tag{6}$$

With $i = X, Z, m$ and $j = Y, l, n$, and M the Mach number.

The model is extended with a model of uncertainties in the stability and control derivatives, the center of gravity and the moments of inertia. The uncertainties in stability and control derivatives are obtained by comparing the aerodynamic models derived using three different methods. The first is Digital Datcom [7] (DDC), a method based on empirical formulas and lookup tables of existing aircraft designs. The second method is Athena Vortex Lattice method [8] (AVL), based on thin airfoil aerodynamic theory using horse shoe vortex computations. The third method is Computational Fluid Dynamics. By comparing the coefficients of these methods a measure of the uncertainties is given. It is assumed that when differences in coefficients between the three methods are small that the coefficient can be determined relatively accurate using simple and fast methods such as AVL and DDC. In the uncertainty model the differences found in the comparison are taken as standard deviations of a normal distribution. Furthermore all aerodynamic uncertainties are assumed to be real parametric uncertainties, hence the uncertainty space is given by Eq. (7)

$$\mathbf{\Delta}_{\text{aero}} := \Delta \in \mathbb{R} | \Delta = N(0, \sigma_{\Delta_k}^2) \tag{7}$$

with subscript k indicating the control or stability derivative. By comparing the derivatives of AVL, DDC, and computational fluid dynamics, it is found that in general the differences in coefficients are within 25%. The uncertainties of C_{Y_β}, C_{Y_p}, C_{L_q}, and C_{m_q} have a standard deviation of 50% and the standard deviation of C_{Y_r} is taken to be 200%. The lift, drag, and moment curve slops coincide very well using the different modeling methods. However the absolute values differ, therefore the lift, drag and moment slope uncertainties are not modeled as percentages but as offsets, having standard deviations of 0.1, 0.02, and 0.2, respectively.

Furthermore, sensor and actuator dynamics are incorporated. Sensor measurements are perturbed by noise and time delay. The noise is modeled as white noise having a sample time of 10 ms. The noise STD for the angular rates is $0.1^\circ/\text{s}$ and 0.25° for the measurement of angle of attack and sideslip. The noise on the angular acceleration measurements of the INDI controller is assumed to be $1^\circ/\text{s}^2$. Actuator dynamics are modeled by actuator rate and position saturations. The control surfaces are assumed to deflect with $150^\circ/\text{s}$ with a maximum of 30°. Control surface deflections are assumed to accurately follow their commands given rate and position saturation. The atmosphere is assumed to be the standard atmosphere without wind.

III. Nonlinear Dynamic Inversion

NDI, also called feedback linearization, is a control strategy that uses the model of a system to control it and through that eliminate the need for gain scheduling and improve performance. In flight control the aerodynamic model of an aircraft is generally used. Fundamental to NDI are the equations of motions (EOM). Knowledge of the different forms of the equations of motion reveals the variety of applications of NDI. This section discusses the theory of basic NDI.

It is assumed that the EOM are affine in the input, Eqs. (8) and (9)

$$\dot{\mathbf{x}} = \mathbf{f}(\mathbf{x}) + \bar{G}(\mathbf{x})\mathbf{u} \tag{8}$$

$$\mathbf{y} = \mathbf{h}(\mathbf{x}) \tag{9}$$

With $\mathbf{x}$ the $n \times 1$ state vector, $\mathbf{u}$ the $m \times 1$ input vector, $\mathbf{y}$ the $m \times 1$ output vector, $\mathbf{f}$ and $\mathbf{h}$ smooth vector fields, and $\bar{G}$ an $n \times m$ matrix whose columns are smooth vector fields. The concept of NDI is to find a direct relation between the desired output and the input and invert it. The dependency is found by differentiating the output until this relation appears. Differentiating the output equation results in Eq. (10)

$$\begin{aligned} \frac{\mathrm{d}\mathbf{h}(\mathbf{x})}{\mathrm{d}t} &= \frac{\partial \mathbf{h}(\mathbf{x})}{\partial \mathbf{x}} \frac{\mathrm{d}\mathbf{x}}{\mathrm{d}t} = \nabla \mathbf{h}(\mathbf{x})\dot{\mathbf{x}} = \nabla \mathbf{h}(\mathbf{x})[\mathbf{f}(\mathbf{x}) + \bar{G}(\mathbf{x})\mathbf{u}] \\ &= \nabla \mathbf{h}(\mathbf{x})\mathbf{f}(\mathbf{x}) + \nabla \mathbf{h}(\mathbf{x})\bar{G}(\mathbf{x})\mathbf{u} = L_f \mathbf{h}(\mathbf{x}) + L_g \mathbf{h}(\mathbf{x})\mathbf{u} \end{aligned} \tag{10}$$

In Eq. (10) $L_f \mathbf{h}(\mathbf{x})$ is called the first-order Lie derivative along the vector field $\mathbf{f}(\mathbf{x})$, defined as $L_f \mathbf{h}(\mathbf{x}) = \nabla \mathbf{h}(\mathbf{x})\mathbf{f}(\mathbf{x})$, with ∇ being the Jacobian operator [1]. $L_g \mathbf{h}(\mathbf{x})$ is the first-order Lie derivative along the vector fields of $\bar{G}(\mathbf{x})$. Assume that the first-order Lie derivative with respect to $\bar{G}(\mathbf{x})$ is not zero. This implies that a relation between the input and the output is found:

$$\dot{\mathbf{y}} = L_f \mathbf{h}(\mathbf{x}) + L_g \mathbf{h}(\mathbf{x})\mathbf{u} \tag{11}$$

The representation is inverted to formulate a control law, Eq. (12). The variable $\dot{\mathbf{y}}$ is replaced by the symbol $\boldsymbol{\nu}$

$$\mathbf{u} = L_g\mathbf{h}(\mathbf{x})^{-1}(\boldsymbol{\nu} - L_f\mathbf{h}(\mathbf{x})) \tag{12}$$

This particular input linearizes the system, resulting into a new system with decoupled dynamics. The linearized system simply results in $\dot{\mathbf{y}} = \boldsymbol{\nu}$, where $\boldsymbol{\nu}$ is called the pseudocontrol input. It is a signal that is tracked by the derivative of the output, hence the output can be controlled by a suitable choice of $\boldsymbol{\nu}$. It is usually obtained using a linear controller, depending on the error, denoted by $\mathbf{e}$, between the controlled parameter and its desired value

$$\boldsymbol{\nu} = (\mathrm{LC})\mathbf{e} \tag{13}$$

If the first-order Lie derivative with respect to $\bar{G}(\mathbf{x})$ would not have been zero, Eq. (10) would be differentiated a second time

$$\begin{aligned}\frac{\mathrm{d}^2h(\mathbf{x})}{\mathrm{d}t^2} &= \frac{\mathrm{d}L_f\mathbf{h}(\mathbf{x})}{\mathrm{d}t} = \frac{\partial L_f\mathbf{h}(\mathbf{x})}{\partial\mathbf{x}}\dot{\mathbf{x}} = \nabla L_f\mathbf{h}(\mathbf{x})[\mathbf{f}(\mathbf{x}) + \bar{G}(\mathbf{x})\mathbf{u}] \\ &= L_f^2\mathbf{h}(\mathbf{x}) + L_gL_f\mathbf{h}(\mathbf{x})\mathbf{u}\end{aligned} \tag{14}$$

With $L_f^2\mathbf{h}(\mathbf{x})$ the second order Lie derivative and $L_gL_f\mathbf{h}(\mathbf{x})$ the first-order Lie derivative of $L_f\mathbf{h}(\mathbf{x})$. If again the Lie derivative with respect to $\bar{G}(\mathbf{x})$ is zero, Eq. (14) is differentiated another time, until the Lie derivative with respect to $\bar{G}(\mathbf{x})$ is nonzero

$$\frac{\mathrm{d}^ih(\mathbf{x})}{\mathrm{d}t^i} = \mathbf{y}^i = L_f^i\mathbf{h}(\mathbf{x}) + L_gL_f^{i-1}\mathbf{h}(\mathbf{x})\mathbf{u} \tag{15}$$

Replacing $\mathbf{y}^i$ by $\boldsymbol{\nu}$, Eq. (15) is inverted to formulate a control law

$$\mathbf{u} = L_gL_f^{i-1}\mathbf{h}(\mathbf{x})^{-1}(\boldsymbol{\nu} - L_f^i\mathbf{h}(\mathbf{x})) \tag{16}$$

Resulting in an ith order closed-loop system $\mathbf{y}^i = \boldsymbol{\nu}$, where the order of the system in this context is the number of times the output equation is differentiated to find a relation between the input and the output.

Up to this point the discussion of NDI has been kept general. To be more specific consider the Euler equations of motion, Eq. (3), for controlling the angular rates of an aircraft, repeated below in vector form.

$$\bar{\mathbf{J}}\dot{\boldsymbol{\omega}} + \boldsymbol{\omega}\times\bar{\mathbf{J}}\boldsymbol{\omega} = \mathbf{M} \tag{17}$$

The angular rates are the controlled variables, $\mathbf{h}(\mathbf{x}) = \boldsymbol{\omega}$. To further specify the control input of an aircraft note that the moment is composed partially by moments generated by the aerodynamics of the airframe (subscript a) and partially by moments generated by the control surface deflections (subscript c)

$$\bar{\mathbf{J}}\dot{\boldsymbol{\omega}} + \boldsymbol{\omega}\times\bar{\mathbf{J}}\boldsymbol{\omega} = \mathbf{M}_a + \mathbf{M}_c \tag{18}$$

$\mathbf{M}_a$ is partially described by multiplication of stability derivatives and the aircraft state ($\mathbf{M}_{a_m}$), taking dimensions into account, Eqs. (5) and (6). And partially by a mismatch between center of gravity and the reference point of the aerodynamic model, multiplied by the aerodynamic forces also described in Eqs. (5) and (6).

$$\mathbf{M}_a = \mathbf{M}_{a_m} + (\mathbf{p}_{\mathrm{ref}} - \mathbf{p}_{\mathrm{CoG}})\times\mathbf{F} \tag{19}$$

To understand the contribution of the second term consider the general aerodynamic model. The model describes the forces and moments that act on the aircraft as a function of aircraft state. It is defined such that all forces act in a specific reference point. Assuming a rigid aircraft, in flight the aircraft motion is described by forces and moments acting in the center of gravity. When using NDI the forces and moments of the aerodynamic model with respect to the reference point have to be translated into forces and moments with respect to the center of gravity, meaning that an extra moment is generated by the forces times the distance between reference point and center of gravity.

The moment that is produced by the control system is a result of the control surfaces generating moments depending on their deflection, which is described by the control derivatives times the deflection of the control surfaces ($\boldsymbol{\delta}$)

$$\bar{\mathbf{J}}\dot{\boldsymbol{\omega}} + \boldsymbol{\omega}\times\bar{\mathbf{J}}\boldsymbol{\omega} = \mathbf{M}_a + (\mathbf{M}_c)_\delta\boldsymbol{\delta} \tag{20}$$

$(\mathbf{M}_c)_\delta$ is given by Eq. (21). Note that here it is assumed that the control derivatives are linear

$$(\mathbf{M}_c)_\delta = \frac{\partial}{\partial\boldsymbol{\delta}}\mathbf{M}_c = \frac{1}{2}\rho V^2S\begin{bmatrix} C_{l_{\delta a}} & 0 & C_{l_{\delta r}} \\ 0 & C_{m_{\delta e}} & 0 \\ C_{n_{\delta a}} & 0 & C_{n_{\delta r}}\end{bmatrix}\begin{pmatrix} b \\ \bar{c} \\ b\end{pmatrix} \tag{21}$$

Solving Eq. (18) for $\dot{\boldsymbol{\omega}}$ yields and expression in the form of Eq. (8)

$$\dot{\boldsymbol{\omega}} = \bar{\mathbf{J}}^{-1}(\mathbf{M}_a + \mathbf{M}_c - \boldsymbol{\omega}\times\bar{\mathbf{J}}\boldsymbol{\omega}) \tag{22}$$

Applying NDI to this equation, Eqs. (10–12) results in an expression for the real input of an aircraft, the control surface deflections $\boldsymbol{\delta}$

$$\boldsymbol{\delta} = (\mathbf{M}_c)_\delta^{-1}(\bar{\mathbf{J}}\boldsymbol{\nu} + \boldsymbol{\omega}\times\bar{\mathbf{J}}\boldsymbol{\omega} - \mathbf{M}_a) \tag{23}$$

The resulting control law depends on the full aerodynamic model contained in M_a and M_c, hence it will depend on all uncertainties of the aerodynamic model. Furthermore it depends on uncertainties in moment of inertia and the center of gravity.

IV. Incremental Nonlinear Dynamic Inversion

NDI in flight control provides the commanded control surface deflections as a function of the error of control variables. At each execution of the flight control laws by the flight control computer, the complete deflection of the control surfaces are computed. As a variation it is possible to only compute the increments of control surface deflections by taking the influence of the acting control surface deflections into account. This concept has been used for the purpose of coping with nonlinear control derivatives, [9]. As demonstrated in this paper, it can also be used to reduce the impact of model mismatch. This approach is fundamentally different from the one discussed by [9]. For use in flight control, it requires rewriting the rotational dynamic equations of motion into an incremental form, which is discussed in this section.

To obtain an incremental form of the dynamic rotational equations of motion, consider a Taylor series expansion of Eq. (22), to obtain a first-order approximation of $\dot{\boldsymbol{\omega}}$ [6]

$$\begin{aligned}\dot{\boldsymbol{\omega}} \approx{}& \bar{\mathbf{J}}^{-1}(\mathbf{M}_{a_0} - \boldsymbol{\omega}_0\times\bar{\mathbf{J}}\boldsymbol{\omega}_0 + \mathbf{M}_{c_0}) \\ &+ \frac{\partial}{\partial\boldsymbol{\omega}}[\bar{\mathbf{J}}^{-1}(\mathbf{M}_a - \boldsymbol{\omega}\times\bar{\mathbf{J}}\boldsymbol{\omega} + \mathbf{M}_c)]_{\boldsymbol{\omega}=\boldsymbol{\omega}_0,\delta=\delta_0}(\boldsymbol{\omega} - \boldsymbol{\omega}_0) \\ &+ \frac{\partial}{\partial\boldsymbol{\delta}}[\bar{\mathbf{J}}^{-1}(\mathbf{M}_a - \boldsymbol{\omega}\times\bar{\mathbf{J}}\boldsymbol{\omega} + \mathbf{M}_c)]_{\boldsymbol{\omega}=\boldsymbol{\omega}_0,\boldsymbol{\delta}=\boldsymbol{\delta}_0}(\boldsymbol{\delta} - \boldsymbol{\delta}_0)\end{aligned} \tag{24}$$

$\boldsymbol{\omega}$ and $\boldsymbol{\delta}$ in Eq. (24) change with time, hence consider $\boldsymbol{\delta}_0$ and $\boldsymbol{\omega}_0$ to be control and state parameters an incremental instance in time before $\boldsymbol{\delta}$ and $\boldsymbol{\omega}$. The first term on the right hand side of Eq. (24) is in fact nothing but $\dot{\boldsymbol{\omega}}_0$

$$\dot{\boldsymbol{\omega}}_0 = \bar{\mathbf{J}}^{-1}(\mathbf{M}_{a_0} - \boldsymbol{\omega}_0\times\bar{\mathbf{J}}\boldsymbol{\omega}_0 + \mathbf{M}_{c_0}) \tag{25}$$

Furthermore, parts of Eq. (24) do not depend on the angular rates and parts do no not depend on the control surface deflection, simplifying Eq. (24) into Eq. (26)

$$\begin{aligned}\dot{\boldsymbol{\omega}} \approx{}& \dot{\boldsymbol{\omega}}_0 + \frac{\partial}{\partial\boldsymbol{\omega}}[\bar{\mathbf{J}}^{-1}(\mathbf{M}_a - \boldsymbol{\omega}\times\bar{\mathbf{J}}\boldsymbol{\omega})]_{\boldsymbol{\omega}=\boldsymbol{\omega}_0,\delta=\delta_0}(\boldsymbol{\omega} - \boldsymbol{\omega}_0) \\ &+ \frac{\partial}{\partial\boldsymbol{\delta}}[\bar{\mathbf{J}}^{-1}\mathbf{M}_c]_{\boldsymbol{\omega}=\boldsymbol{\omega}_0,\boldsymbol{\delta}=\boldsymbol{\delta}_0}(\boldsymbol{\delta} - \boldsymbol{\delta}_0)\end{aligned} \tag{26}$$

Equation (26) can be simplified even further, when noting that for an incremental time advance the second term on the right hand side is

much smaller than the third term. This is explained as follows. A change in control input has a change in moment as effect. The change in moment is directly effecting the angular accelerations. On the other hand, the angular rates only change by integrating the angular accelerations, hence by integrating the control surface deflection component. Which makes the $(\boldsymbol{\omega} - \boldsymbol{\omega}_0)$ component, the change in angular rates, negligible for small time increments. Note that here it is assumed that a demanded deflection is achieved instantaneous, Eq. (27)

$$\dot{\boldsymbol{\omega}} = \dot{\boldsymbol{\omega}}_0 + \frac{\partial}{\partial \boldsymbol{\delta}}[\bar{\mathbf{J}}^{-1}\mathbf{M}_c]_{\omega=\omega_0,\delta=\delta_0}(\boldsymbol{\delta} - \boldsymbol{\delta}_0) \tag{27}$$

Assuming a linear relation between control deflection and control moment, Eq. (24) can finally be rewritten into Eq. (28)

$$\dot{\boldsymbol{\omega}} = \dot{\boldsymbol{\omega}}_0 + \bar{\mathbf{J}}^{-1}(\mathbf{M}_c)_\delta \, \mathrm{d}\boldsymbol{\delta} \tag{28}$$

Equation (28) is a linear approximation of Eq. (17) around $\boldsymbol{\delta}_0$ and $\boldsymbol{\omega}_0$ for small time increments, describing the changes in angular accelerations as a function of control increments. The new representation of the dynamic rotational equations of motion contains three significant implications. First of all, the aerodynamic moment term $\mathbf{M}_a$ has disappeared from the equation, hence the angular acceleration is not expressed in terms of the largest part of the aerodynamic model any more. Second, the $\mathbf{M}_a$ term also depends on the location of the center of gravity through the definition of the aerodynamic model, hence this dependency is also eliminated. And third, the expression does not contain the nonlinear cross couplings of angular rates, $\boldsymbol{\omega} \times \bar{\mathbf{J}}\boldsymbol{\omega}$.

Using the newly found equation for the rotational dynamics the general NDI procedure [Eqs. (10–12)] is applied. Define the parameter to be controlled as the angular rates. Hence the output equation is given by

$$\mathbf{y} = \mathbf{h}(\mathbf{x}) = \boldsymbol{\omega} \tag{29}$$

To obtain a relation with the input, the output is differentiated

$$\dot{\mathbf{y}} = \dot{\boldsymbol{\omega}} = \dot{\boldsymbol{\omega}}_0 + \bar{\mathbf{J}}^{-1}(\mathbf{M}_c)_\delta \, \mathrm{d}\boldsymbol{\delta} \tag{30}$$

The direct relation to the input is found after differentiating once. Replacing the angular acceleration by the pseudocontrol input $\boldsymbol{\nu} = \dot{\boldsymbol{\omega}}$, the linearizing control input Eq. (31) is found by inverting Eq. (30)

$$\mathrm{d}\boldsymbol{\delta} = (\mathbf{M}_c)_\delta^{-1}\bar{\mathbf{J}}(\boldsymbol{\nu} - \dot{\boldsymbol{\omega}}_0) \tag{31}$$

Note that this control law results in control surface deflection changes. These changes must be added to the current deflections to obtain the full new control surface deflections. For practical implementation in the system described by Eq. (8) this last step must be added, Eq. (32)

$$\mathbf{u} = \boldsymbol{\delta} = \boldsymbol{\delta}_0 + \mathrm{d}\boldsymbol{\delta} \tag{32}$$

Applying NDI to the incremental form of the equations of motion, referred to from here on as incremental NDI (INDI), results in a control law that is not depending on the largest part of the aerodynamic model , hence it is not effected by the largest part of the aerodynamic uncertainties. This increases the robustness of the system as is discussed in the next section.

V. Uncertainties

The aircraft dynamics are considered to be nonlinear and as shown, using NDI, a linearizing control law can be designed. Resulting in a linear and time invariant closed-loop system. However as will be demonstrated the linearizing control law resulting from NDI is not completely linearizing anymore under the influence of uncertainties, as has been shown by [3]. On the other hand, the linearizing control law resulting from INDI remains linearizing. To demonstrate the influence of uncertainties the general system description as given by Eq. (8) is reformulated, Eq. (33)

$$\dot{\mathbf{x}} = \mathbf{f}_n(\mathbf{x}) + \bar{G}_n(\mathbf{x})\mathbf{u} \tag{33}$$

Subscript n is added to indicate the nominal situation. If no uncertainties exist this is the real system. Continuing along the general NDI procedures (10–12), a linearizing control law is found. For simplicity a first-order system is assumed

$$\mathbf{u} = L_g\mathbf{h}(\mathbf{x})^{-1}(\boldsymbol{\nu} - L_f\mathbf{h}(\mathbf{x})) = \bar{G}_n^{-1}(\boldsymbol{\nu} - \mathbf{f}_n(\mathbf{x})) \tag{34}$$

resulting in the closed loop

$$\dot{\mathbf{x}} = \boldsymbol{\nu} \tag{35}$$

In reality uncertainties do exist, hence the representation of Eq. (33) is not complete. Equation (33) must be seen as the system known by the Flight Control Computer (FCC) or the system the FCC believes to be the real system. The true system is represented as the system known by the FCC plus an additional, not known, hence uncertain part

$$\dot{\mathbf{x}} = \mathbf{f}_n(\mathbf{x}) + \Delta\mathbf{f}(\mathbf{x}) + \bar{G}_n(\mathbf{x})\mathbf{u} + \Delta\bar{G}(\mathbf{x})\mathbf{u} \tag{36}$$

Application of NDI to the true system, Eq. (36), means that the input, $\mathbf{u}$, is defined as in (34), the linearizing control law for the system as known by the FCC. The resulting closed-loop system is analytically derived by substituting the linearizing control law into the real system [3]

$$\begin{aligned}
\dot{\mathbf{x}} &= \mathbf{f}_n(\mathbf{x}) + \Delta\mathbf{f}(\mathbf{x}) + \bar{G}_n(\mathbf{x})[\bar{G}_n^{-1}(\boldsymbol{\nu} - \mathbf{f}_n(\mathbf{x}))] \\
&\quad + \Delta\bar{G}(\mathbf{x})[\bar{G}_n^{-1}(\boldsymbol{\nu} - \mathbf{f}_n(\mathbf{x}))] \\
\dot{\mathbf{x}} &= \boldsymbol{\nu} + \Delta\mathbf{f}(\mathbf{x}) + \Delta\bar{G}(\mathbf{x})\bar{G}_n^{-1}\boldsymbol{\nu} - \Delta\bar{G}(\mathbf{x})\bar{G}_n^{-1}\mathbf{f}_n(\mathbf{x}) \\
\dot{\mathbf{x}} &= [\Delta\mathbf{f}(\mathbf{x}) - \Delta\bar{G}(\mathbf{x})\bar{G}_n^{-1}\mathbf{f}_n(\mathbf{x})] + [I + \Delta\bar{G}(\mathbf{x})\bar{G}_n^{-1}]\boldsymbol{\nu}
\end{aligned} \tag{37}$$

This is not necessarily a linear equation anymore, such as Eq. (35). In particular for angular rate control of aircraft using regular NDI the closed-loop system expressed by Eq. (37) is given by Eq. (38), when assuming negligible measurement uncertainties

$$\begin{aligned}
\dot{\boldsymbol{\omega}} &= [\Delta\bar{\mathbf{J}}^{-1}\Delta\mathbf{M}_a - \Delta\bar{\mathbf{J}}^{-1}(\omega\times\bar{\mathbf{J}}\omega) \\
&\quad - \Delta\bar{\mathbf{J}}^{-1}\Delta\mathbf{M}_c\mathbf{M}_{c_n}^{-1}\bar{\mathbf{J}}(\mathbf{M}_a - \omega\times\bar{\mathbf{J}}\omega)] + [I + \Delta\bar{\mathbf{J}}^{-1}\Delta\mathbf{M}_c\mathbf{M}_{c_n}^{-1}\bar{\mathbf{J}}]\boldsymbol{\nu}
\end{aligned} \tag{38}$$

Here $\Delta\mathbf{M}_a$ contains uncertainties in center of gravity (CG) and all aerodynamic uncertainties in terms of stability derivatives. $\Delta\mathbf{M}_c$ contains uncertainties in control derivatives. $\Delta\bar{\mathbf{J}}$ represents uncertainties in the moments of inertia. Also the nonlinear cross product of the angular rates, $\boldsymbol{\omega} \times \bar{\mathbf{J}}\boldsymbol{\omega}$, remain in the equation.

Now consider INDI. Recall the derivation of the general incremental representation of the equations of motion, Eqs. (24–28), with $\dot{\boldsymbol{\omega}}_0$ assumed to be measurable

$$\dot{\mathbf{x}} = \mathbf{f}_n(\mathbf{x}) + \bar{G}_n(\mathbf{x})\mathbf{u} \qquad \dot{\boldsymbol{\omega}} = \dot{\boldsymbol{\omega}}_0 + \bar{\mathbf{J}}^{-1}(\mathbf{M}_c)_\delta \, \mathrm{d}\boldsymbol{\delta} \tag{39}$$

Note that here $\mathbf{f}_n(\mathbf{x})$ represents $\dot{\boldsymbol{\omega}}_0$ and not $\mathbf{M}_a$. This is an important difference, because $\dot{\boldsymbol{\omega}}_0$ is a measurements, whereas $\mathbf{M}_a$ depends on model parameters. When the angular accelerations are assumed to be known accurately, hence again that measurement uncertainties are negligible, the real world representation is slightly different from Eq. (36). The term $\Delta\mathbf{f}_n(\mathbf{x})$ does not appear in Eq. (40)

$$\dot{\mathbf{x}} = \mathbf{f}_n(\mathbf{x}) + \bar{G}_n(\mathbf{x})\mathbf{u} + \Delta\bar{G}(\mathbf{x})\mathbf{u} \tag{40}$$

Applying INDI, Eq. (31), to the linearized approximation of the true system results in Eq. (41)

$$\begin{aligned}
\dot{\mathbf{x}} &= \mathbf{f}_n(\mathbf{x}) + \bar{G}_n(\mathbf{x})[\bar{G}_n^{-1}(\boldsymbol{\nu} - \mathbf{f}_n(\mathbf{x}))] + \Delta\bar{G}(\mathbf{x})[\bar{G}_n^{-1}(\boldsymbol{\nu} - \mathbf{f}_n(\mathbf{x}))] \\
\dot{\mathbf{x}} &= -\Delta\bar{G}(\mathbf{x})\bar{G}_n^{-1}\mathbf{f}_n(\mathbf{x}) + (I + \Delta\bar{G}(\mathbf{x})\bar{G}_n^{-1})\boldsymbol{\nu} \\
\dot{\boldsymbol{\omega}} &= -\Delta\bar{\mathbf{J}}^{-1}\Delta\mathbf{M}_c\mathbf{M}_{c_n}^{-1}\bar{\mathbf{J}}\dot{\boldsymbol{\omega}}_0 + [I + \Delta\bar{\mathbf{J}}^{-1}\Delta\mathbf{M}_c\mathbf{M}_{c_n}^{-1}\bar{\mathbf{J}}]\boldsymbol{\nu} \\
\dot{\boldsymbol{\omega}} &= -B\dot{\boldsymbol{\omega}}_0 + (I + B)\boldsymbol{\nu}
\end{aligned} \tag{41}$$

For simplicity the new notation $B = \Delta\bar{\mathbf{J}}^{-1}\Delta\mathbf{M}_c\mathbf{M}_{c_n}^{-1}\bar{\mathbf{J}}$ is introduced. Equation (41) is a linear system with uncertainties in the control derivatives and moments of inertia. The block diagram of this process is illustrated in Fig. 1. With $\boldsymbol{\omega}_0$ the integrated $\dot{\boldsymbol{\omega}}$ and $\dot{\boldsymbol{\omega}}_0$ the derivative of $\boldsymbol{\omega}_0$.

The corresponding transfer function of Fig. 1 is given by Eq. (43), which states that through using INDI the uncertainties in the system are eliminated. As long as the sign of the control derivatives is known and assuming instant deflections and measurable angular accelerations

$$FF = K(I+B)\frac{I/s}{I+sB/s} = K\frac{I+B}{s(I+B)} = \frac{K}{s} \tag{42}$$

$$\frac{\Omega}{\Omega_{\text{ref}}} = \frac{FF}{I+FF} = \frac{K/s}{I+K/s} = \frac{K}{s+K} \tag{43}$$

with $\Omega(s)$ being the Laplace transform of ω. Recall that B contains uncertainties in control derivatives and moment of inertia matrix. In addition the dependency on the center of gravity and other aerodynamic derivatives is eliminated since the effect is captured by the measured angular accelerations. Hence using INDI the control system is insensitive to uncertainties in aerodynamic model, center of gravity and moment of inertia. When a proportional controller is selected to close the loop, the closed-loop transfer function of the linearized system is given by a simple first-order low-pass filter, as it would be the case for regular NDI without any uncertainties in the system.

To understand the limitations of the derivation and the applicability in practice, the assumptions that result in this conclusion and the implications are repeated and discussed. Three assumptions are made for INDI:

1) The first assumption is that the second term on the right hand side of Eq. (26) is negligible. If taken into account, this term could be added in Eq. (41) as an extra uncertainty, which would include all the uncertainties of the aerodynamic stability derivatives and the center of gravity. However, as mentioned before, the change in angular rates for small time increments is small by definition, since the angular rates are an integrated consequence of the control surface deflections. Again note that for this assumption to be true instantaneous control surface deflections are implied.

2) Hence the second assumption, ideal actuators; actuator dynamics are not taken into account in the derivation. Instantaneous deflections are assumed in the derivation, justifying the claim that the second term on the right hand side of Eq. (26) can be neglected. In practice deflections are not achieved instantaneous, however, actuator deflections are fast. The UAV considered in this paper achieves values of 150 deg/s. If the demanded control surface deflections result in actuator saturation, through a suitable choice of control gain the control surface commands can be accelerated or decelerated, which sppeds the system up or slows it down.

3) Ideal sensors; up to this point the angular accelerations have simply been assumed to be known without error. Angular acceleration sensors exist, however, they are not common. Alternatively the angular accelerations can be derived from inertial measurement unit (IMU) gyro measurements. In any case, the measurements will contain biases, noise and measurement delay.

Uncertainties in the form of biases can be compensated by outer loops. INDI should work for common and cheap systems, hence using an IMU with high noise levels and not angular acceleration sensors. The IMU sensor noise in that case, however, eliminates the option of numeric differentiation, because it is generally known to cause problems. Time delay, depending on the filtering and processor capabilities, is in the order of milliseconds, however, from simulations it is observed that even small measurement delays are of significant concern when using INDI. Because by using INDI the demanded angular acceleration is considered to be an incremental step in time from the measured angular acceleration, any noticeable delay will violate the assumption of the incremental step, hence causing loss of performance. Concluding, the assumption of ideal sensors does not hold in practice. The angular acceleration measurements are not available and the time delay cannot be zero.

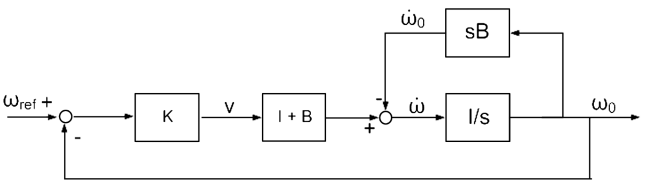

Fig. 1 Block diagram of the closed-loop system using INDI.

VI. Prediction

To understand the problem caused by time delay of real world sensors, consider the linearizing control law for INDI [Eq. (31)]

$$\mathrm{d}\,\boldsymbol{\delta} = (\mathbf{M}_c)_\delta^{-1}\bar{\mathbf{J}}(\boldsymbol{\nu} - \dot{\boldsymbol{\omega}}_0)$$

When subject to time delay, the measured angular accelerations are delayed, denoted by $\boldsymbol{\omega}_\tau$

$$\mathrm{d}\,\boldsymbol{\delta} = (\mathbf{M}_c)_\delta^{-1}\bar{\mathbf{J}}(\boldsymbol{\nu} - \dot{\boldsymbol{\omega}}_\tau) \tag{44}$$

When using this as input to the system, not all terms are canceled

$$\dot{\boldsymbol{\omega}} = \dot{\boldsymbol{\omega}}_0 + \bar{\mathbf{J}}^{-1}(\mathbf{M}_c)_\delta(\mathbf{M}_c)_\delta^{-1}\bar{\mathbf{J}}(\boldsymbol{\nu} - \dot{\boldsymbol{\omega}}_\tau)$$
$$\dot{\boldsymbol{\omega}} = \boldsymbol{\nu} + \dot{\boldsymbol{\omega}}_0 - \dot{\boldsymbol{\omega}}_\tau = \boldsymbol{\nu} + \dot{\boldsymbol{\omega}}_{\Delta\tau} \tag{45}$$

Equation (45) shows that the closed-loop system is not linearized completely. An extra term remains that is varying with time, $\dot{\boldsymbol{\omega}}_{\Delta\tau}$. $\dot{\boldsymbol{\omega}}_{\Delta\tau}$ is the difference of the angular accelerations at two different instances in time. As the time delay is decreased the influence of $\dot{\boldsymbol{\omega}}_{\Delta\tau}$ becomes smaller, up to a time delay of zero.

Because it is impossible to eliminate the time delay, the control system must be adjusted to anticipate upon it, which can be done using a predictive filter. Required is that the error in predicted angular acceleration is small enough such that it can be neglected. In [10–13] several methods to predict angular acceleration have been proposed. These methods are, however, rather complex, varying from multiple neural networks to extensive Kalman filtering. The present situation can be simplified such that complex predictive filters are not required.

Because INDI decouples the dynamics of the controlled aircraft, it is justified to design a decoupled predictive filter. For example, a filter to predict the pitch angular accelerations uses only longitudinal parameters, and similar for roll and yaw angular acceleration prediction.

For the prediction of the angular acceleration several parameters qualify, such as the current angular acceleration, the control surface deflections, the angular rates and the angular rate references. The drawbacks of angular acceleration in terms of availability and noise have already been discussed. Regarding control surface deflections it is noted that they are aircraft dependent. For each aircraft the control surface deflection to create an angular acceleration will be different. The deflection depends on the aircraft moment of inertia and control derivatives, which again depend on wing shape and control surface sizing. With the objective of obtaining a generic control law, the two parameters remaining that should be used are the angular rates and the references thereof.

The predictive filter must predict the closed-loop response of the controller and the aircraft. Because for INDI the closed-loop response is known and simple regardless of uncertainties, Eq. (43), a simple linear filter can be designed using the closed-loop model. An advantage of linear prediction is that bounded-input bounded-output stability is guaranteed. In Eq. (46) the expression for the chosen linear predictive filter is given

$$\dot{\omega}_{(t)} = \sum_{i=1}^{5}[\theta_{\omega_j}\omega_{(t-i\,\mathrm{d}t)} + \theta_{r_j}r_{(t-i\,\mathrm{d}t)}] + \epsilon \tag{46}$$

with r_j the reference angular rate with j for the roll, pitch, and yaw rate. The coefficients (θ) of the predictive filter are computed using

least squares estimation, which requires a data set to estimate coefficients. Least squares estimation solves the overdetermined system Eq. (47) for θ using a cost function, Eq. (48). H contains collected data of the angular rates and the angular rate references, and z contains data of the predicted angular accelerations, hence one time step ahead ($i = 0$)

$$z = H\theta + \epsilon \tag{47}$$

$$J = \frac{1}{2}\sum_{k=1}^{N}\epsilon_k^2 = \frac{1}{2}(z - H\theta)^T(z - H\theta) \tag{48}$$

$$\frac{\partial J}{\partial \theta} = H^T(z - H\theta) = 0 \tag{49}$$

$$\theta = (H^T H)^{-1}H^T z \tag{50}$$

To maximally use INDI, it is crucial to obtain the data in a generic fashion. Because a closed-loop system controlled with INDI is model independent, the general closed-loop system, Eq. (43) can be used for that purpose. Data is generated from a simulation of a low-pass filter response to a single step input. Using least squares estimation on the generated data ideal coefficients are computed. Hence the predictive filter is constructed without prior knowledge of the aircraft model or availability of test data.

The sample rate of the generated data must be chosen equal to the sample rate of the flight control computer. Otherwise the predicted value becomes too large or too small. It is important to understand that the predictive filter only works in combination with INDI itself. This combination is from here on referred to as predictive incremental nonlinear dynamic inversion (PINDI).

The magnitude of the step exciting the low-pass filter is taken to be 10 rad/s for all three rates. Note that this approach results in the same coefficients for all three predictive filters of the three angular rates. The ideal coefficients are given in Table 1.

To understand why the predictive filter will not cause problems with sensor noise, compare the predictive filter to a numeric differentiation scheme. The difference is shown by comparing the predictive filter coefficients to numerical differentiation scheme coefficients. As an example the five point numerical scheme is given by Eq. (51), [14]. The coefficients multiplying the angular rates at different sample times are much larger than the coefficients given by Table 1. Lower-order schemes, such as the three point scheme and Euler differentiation, may reduce the noise generated by differentiation, but they will also be less accurate and furthermore will not contain less noise than the predictive filter

$$\dot{\omega}_t = -\frac{1}{12\mathrm{d}t}[-25\omega_t + 48\omega_{t-\mathrm{d}t} - 36\omega_{t-2\,\mathrm{d}t} + 16\omega_{t-3\,\mathrm{d}t} - 3\omega_{t-4\,\mathrm{d}t}] \tag{51}$$

VII. Outer Loop Control Laws

To test the control system performance, test cases for the controllers consist of step inputs on the pitch rate (q) and the roll rate (p). The yaw rate is chosen by an outer loop control law, such that the sideslip angle is minimized. The outer loop controller uses the time scale separation principle [12]. The time scale separation principle uses the fact that the time constants of the inner and outer loops are different and hence the control laws for inner and outer loops can be designed independent. For completeness the control law for the sideslip is given below. Finally note that the thrust is controlled to maintain constant airspeed, which will not be treated in this paper.

Table 1 Ideal coefficients used in the predictive filter

Coefficient	Value	Coefficient	Value
$\theta_{r_{t-1\,\mathrm{d}t}}$	4.8771	$\theta_{\omega_{t-1\,\mathrm{d}t}}$	−0.8058
$\theta_{r_{t-2\,\mathrm{d}t}}$	−0.1986	$\theta_{\omega_{t-2\,\mathrm{d}t}}$	−0.8369
$\theta_{r_{t-3\,\mathrm{d}t}}$	−0.1481	$\theta_{\omega_{t-3\,\mathrm{d}t}}$	−0.8723
$\theta_{r_{t-4\,\mathrm{d}t}}$	−0.0983	$\theta_{\omega_{t-4\,\mathrm{d}t}}$	−0.9119
$\theta_{r_{t-5\,\mathrm{d}t}}$	−0.0490	$\theta_{\omega_{t-5\,\mathrm{d}t}}$	−0.9562

β is chosen to be a control variable since it is otherwise difficult to find a reference for the yaw rate. The reference sideslip angle is set to zero in all situations. To do so, an expression for $\dot{\beta}$ is derived by differentiating the expression for the sideslip angle, Eq. (52) and rewriting it with substitution of Eq. (1) [15]

$$\beta = \sin^{-1}\frac{v}{V} \tag{52}$$

$$\dot{\beta} = \frac{1}{\sqrt{V^2 - v^2}}(F_X + F_Y + F_Z) + \begin{bmatrix} \frac{w}{\sqrt{V^2-v^2}} & 0 & \frac{-u}{\sqrt{V^2-v^2}} \end{bmatrix}\begin{bmatrix} p \\ q \\ r \end{bmatrix} \tag{53}$$

$$F_X = -\frac{uv}{V^2}[-g\sin\theta + a_x]$$

$$F_Y = \left(1 - \frac{v^2}{V^2}\right)[g\sin\psi\cos\theta + a_y]$$

$$F_Z = -\frac{vw}{V^2}[g\cos\psi\cos\theta + a_z]$$

with a_i the acceleration along i, and with $i = x, y, z$ being the three-body fixed axes. Inverting this equation results in an expression for the yaw rate reference signal, as a function of the pseudocontrol input for $\dot{\beta}$, which is provided by another linear controller. And as a function of the roll and pitch rate reference signals

$$r_{\mathrm{ref}} = \left(\frac{-u}{\sqrt{V^2 - v^2}}\right)^{-1}\left[\nu_\beta - \frac{1}{\sqrt{V^2 - v^2}}(F_X + F_Y + F_Z) - \begin{bmatrix} \frac{w}{\sqrt{V^2-v^2}} & 0 \end{bmatrix}\begin{bmatrix} p_{\mathrm{ref}} \\ q_{\mathrm{ref}} \end{bmatrix}\right] \tag{54}$$

VIII. Results

The robust performance of three control systems in angular rate reference tracking is compared in simulations using Matlab/Simulink. One uses NDI, one INDI and the third uses PINDI. The INDI controller assumes the direct measurement of angular accelerations without delay, making the INDI controller a hypothetical controller. The NDI and PINDI controller on the other hand are controllers that can be implemented in aircraft with a commonly used set of sensors, in particular an IMU, angle of attack and sideslip sensor and a pitot static tube for true airspeed.

All simulations are performed with actuator dynamics in the form of position and speed saturation and a measurement delay of 10 ms for the NDI and PINDI controllers and zero time delay for the INDI controller, except when mentioned otherwise. The control system is updated at 100 Hz, hence the time delay is equal in size to the control update time step. All simulations are performed with a fixed sample frequency, also equal to 100 Hz. Furthermore all linear controllers generating the pseudocontrol inputs are proportional controllers only, except for the inner loop NDI control. The gains are given in Table 2. The step inputs used to compute the coefficients of the predictive filter are different from those used to determine the predictive filter coefficients both in magnitude and sign. Furthermore the simulation does not contain a trimming routine, hence initial divergence from reference parameters is caused by untrimmed initial conditions. The simulations are all performed at 34 m/s and flight at sea level.

The robust performance of the three control systems is investigated by consequently varying sources of uncertainty while using the same step inputs on the roll and pitch rate and minimizing

Table 2 Linear controller gains

Coefficient	NDI	INDI	PINDI
Roll rate proportional gain	10	5	5
Roll rate integrational gain	5	0	0
Pitch rate proportional gain	10	5	5
Pitch rate integrational gain	5	0	0
Yaw rate proportional gain	10	5	5
Yaw rate integrational gain	5	0	0
Roll angle proportional gain	2	2	2
Pitch angle proportional gain	2	2	2
Sideslip angle proportional gain	2	2	2

the sideslip angle. The sources of uncertainty are the aerodynamic model, the center of gravity, the moment of inertia and the sensor measurements in terms of noise.

Figures 2a and 2b present the nominal response of the closed-loop systems. Each of the controllers track the step inputs satisfactory. The response of the NDI controller is fastest, with a rise time of 0.2 s and an overshoot of 7%. The INDI controller does not experience any overshoot and has a rise time of 0.5 s. The rise time of the PINDI controller is around 0.35 s without any overshoot. In the longitudinal response of the PINDI system it is noted that the longitudinal motion is influenced marginally by the lateral dynamics.

Figures 2c and 2d present the sideslip angle response and the true and predicted angular accelerations of the predictive filter, respectively. These two plots are only presented for the nominal response because their characteristics vary analogously to the rate responses. For each step input it is observed that initially the predicted angular acceleration is larger than the true value. This is an indication of the control surface rate saturation. Because the ideal closed-loop response assumes instantaneous deflections the predicted accelerations are too high. This also causes the transient response in Fig. 2b. A high angular acceleration prediction does not cause the system to become unstable because it results in smaller deflections, hence adding a damping effect to the system.

The mismatch observable in Fig. 2d between true and predicted yaw acceleration is caused by a changing yaw rate reference. During a roll rate step input, the aircraft is linearly increasing its bank angle. In a coordinated turn, hence a turn without sideslip, a fixed bank angle corresponds to a constant yaw rate. For a changing bank angle, the corresponding yaw rate is also changing. Because the closed-loop rate controlled response is that of a first-order system a lag error is present as seen in Fig. 2d.

In Fig. 3 the nominal response of the INDI with a 10 ms measurement delay is presented. For comparison the nominal responses of the NDI and the PINDI system are repeated. The oscillation that is noticeable in Fig. 3 is caused by $\dot{\boldsymbol{\omega}}_{\Delta\tau}$ of Eq. (45), which is constantly varying in magnitude. The response of the PINDI controller clearly

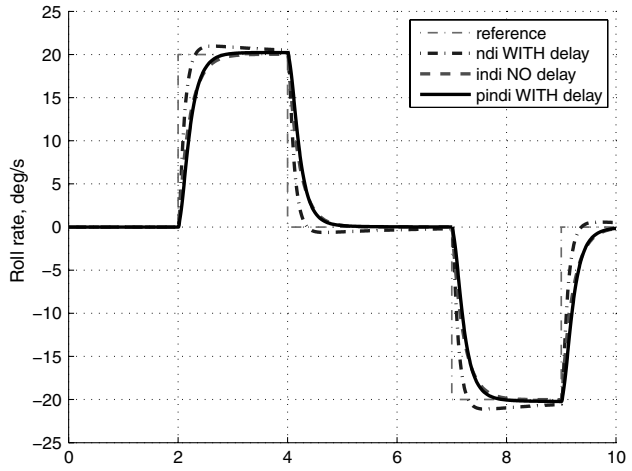

a) Roll rate

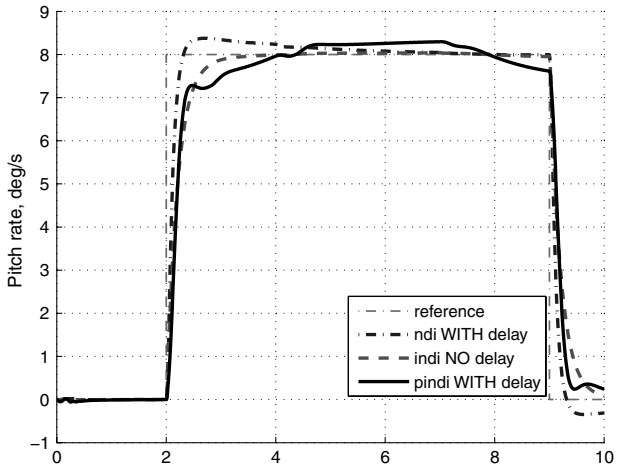

b) Pitch rate

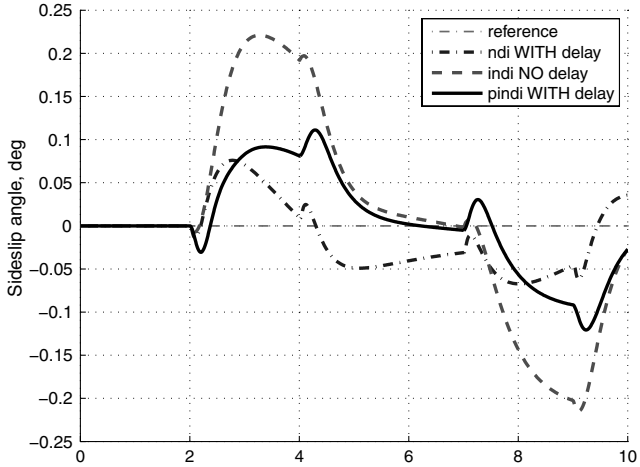

c) Sideslip angle

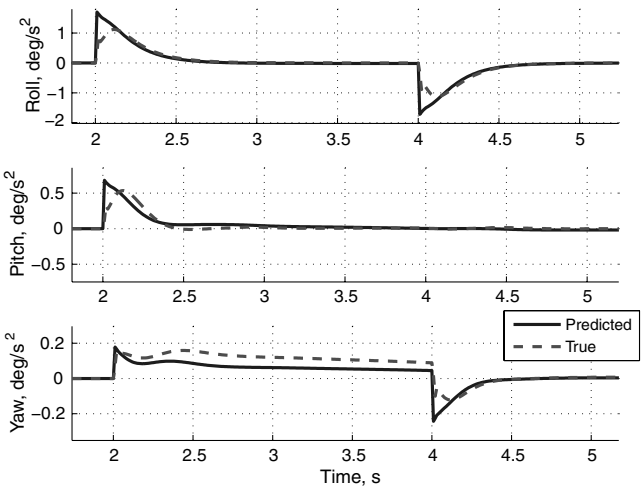

d) Predicted and true angular acceleration

Fig. 2 The nominal response of the UAV controlled using NDI, INDI, and PINDI. The NDI and PINDI controllers are subject to sensor measurement time delays of 10 ms, and the INDI controlled system is not.

illustrates the effect of adding the predictive filter. The oscillations vanish and the response is satisfactory.

Figures 4 and 5 show the performance subject to aerodynamic model mismatch. The aerodynamic mismatches are present both in the stability and control derivatives hence in $\mathbf{M}_a$ and $\mathbf{M}_c$. Note once more that the responses of the NDI and the PINDI controller are with time delays on the measurements and the INDI response is without time delay in the measurement. In the simulation of Fig. 4, the responses to five realizations of the uncertainty space described in Sec. II are presented. The conventional NDI controller suffers from the model mismatch. The responses are different for each realization and the performance is unsatisfactory, with overshoots of 50% or with responses not reaching the reference value.

The response of the INDI controller does not show any sensitivity to the aerodynamic model mismatch, not to the stability nor the control derivatives mismatches. The responses are nearly identical to those of the nominal simulation. Compared with the ideal INDI controlled system, the PINDI controller responds marginally worse. It is observed that the steady-state error remains uninfluenced by the uncertainties. Merely the response time of the system is changed by a fraction of a second and the influence of the lateral motion on the longitudinal response has increased marginally. The larger influence to model inaccuracies of the PINDI controller compared with the INDI controller is explained by the angular acceleration prediction, which computes angular accelerations based on ideal coefficients that are always marginally off. Because the aircraft models are varied in the simulations, the error is different in each realization. However, compared with conventional NDI the response of PINDI is a significant improvement.

Figure 5 presents results of a Monte–Carlo simulation containing 1000 samples of the aerodynamic model. The two graphs show the rms error of the angular rates compared with the nominal response. The few larger rms errors shown in the box plots of INDI and PINDI are explained by long term actuator saturation, caused by physically impossible demands to the aircraft motion in the present flight conditions. Because in the simulations all uncertainties are added in the model instead of in the control system airplane models occur that are physically not capable of following the step inputs of the angular rates.

Figure 6 shows the results of a simulation with a mismatch in center of gravity. The mismatch is taken to be 50% of the mean aerodynamic chord both along the aircraft x and z axis, moving the center of gravity further to the rear of the aircraft. The moment of inertia change caused by the shift of center of gravity is negligible. The results clearly indicate that conventional NDI cannot cope with a mismatch in center of gravity, whereas the responses of the INDI and

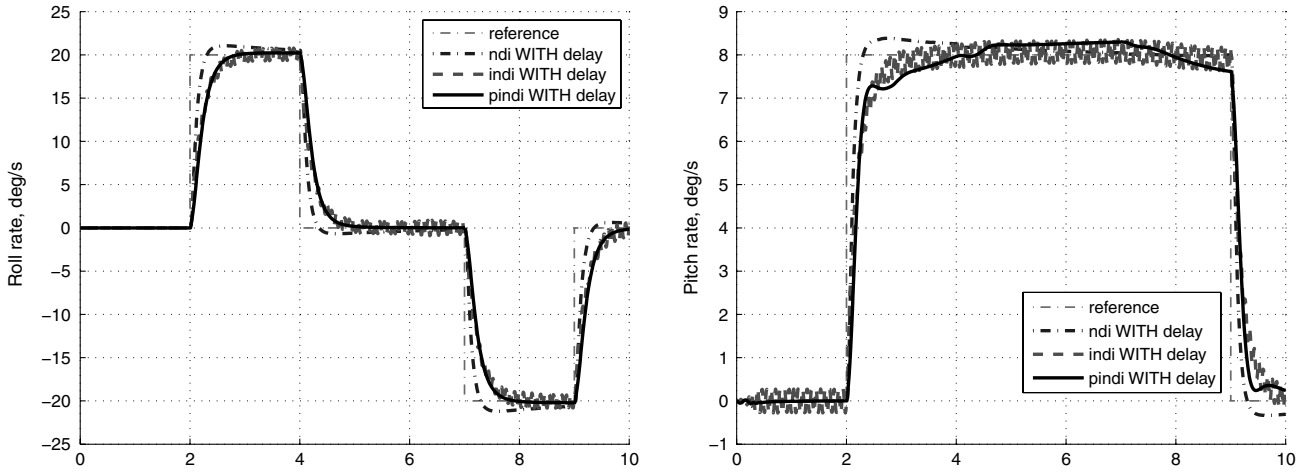

a) Roll rate b) Pitch rate

Fig. 3 The inner loop nominal response of the UAV controlled using NDI, INDI, and PINDI. All three control systems are subject to sensor measurement time delays of 10 ms.

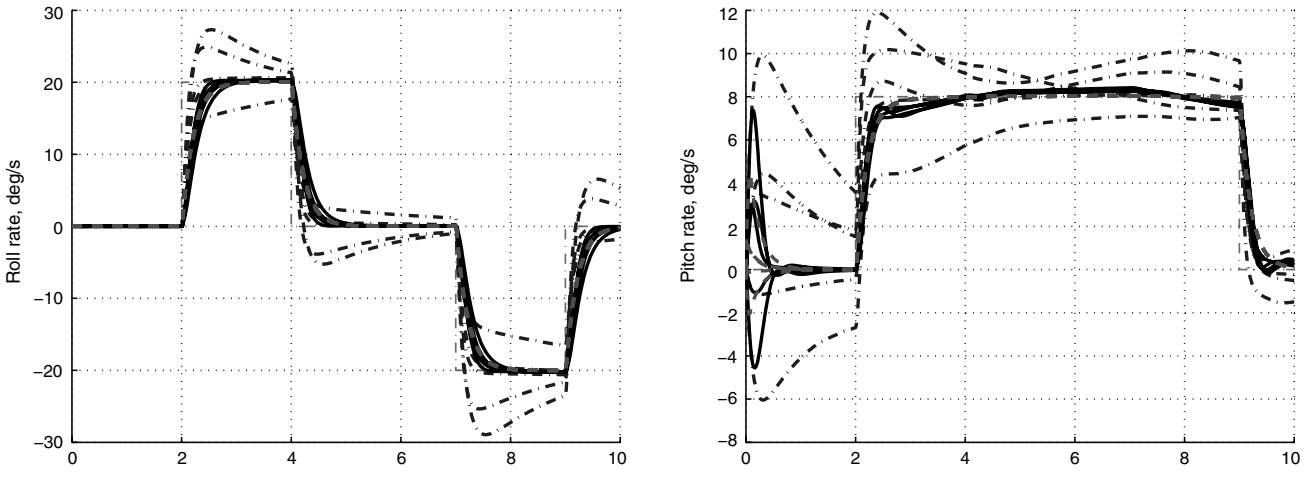

a) Roll rate, deg/s b) Pitch rate, deg/s

Fig. 4 The inner loop response of the UAV controlled using NDI, INDI, and PINDI, subject to mismatches in the aerodynamic model, both in stability and control derivatives. The NDI and PINDI controllers are subject to sensor measurement time delays, and the INDI controlled system is not.

PINDI systems are, respectively, not and slightly different from their nominal responses. The PINDI controller has a well-damped 20% overshoot, and a settling time of within 1 s.

In Fig. 7 the responses with a 50% mismatch in moment of inertia is presented, meaning that the inertia in the FCC is twice the actual size. The mismatch in inertia causes the computed control surface deflections to be larger or smaller than required for the desired maneuver with a magnitude directly proportional to the mismatch, Eq. (31). The conventional NDI controlled system is influenced only marginally by the mismatch. The influence is marginal because conventional NDI calculates the control deflections from flight parameters that are related to the angular acceleration by integrating once and twice, which has a damping effect. INDI on the other hand derives the deflections directly from angular accelerations, without any damping causing the control system to constantly overshoot the desired angular rate. Note, however, that apart from the oscillations the reference signal is tracked. The fact that PINDI does not suffer from overshoots is caused by the predictive filter which again has a damping effect, since the ideal coefficients do not anticipate on the faster response of the system and predict angular accelerations that are smaller than the true values.

Figure 8 shows the responses to sensor noise. From the responses it is noted that for non of the controllers the noise is blown up and causing significant loss of performance. The NDI response is satisfactory. The noise is clearly noticeable, but the response is similar to the nominal response. The INDI controller also responds satisfactory to noise. The noise on the PINDI system response is of the same magnitude as for the NDI controller system. Note that the noise in the PINDI system is not blown up, which is generally known to cause problems when numerically differentiating noisy signals. Because PINDI uses prediction instead of numerical differentiation, this is not a problem.

IX. Discussion

The crux of INDI and PINDI is that almost all model uncertainties that degrade the performance of regular NDI are replaced by a (indirect) measurement. This includes the nonlinear effects of the angular rate cross product. The resulting control law does therefore not depend on the greatest part of the model ($\mathbf{M}_a$), resulting in responses that are non model dependent to a large degree.

The reason that the PINDI controller is sensitive to the model uncertainties to a slightly larger degree than the INDI controller is that the predictive filter is designed for an aircraft with an ideal response. Because instant control surface deflections are assumed in the derivation and because contributions to the angular accelerations other than control surface deflections are neglected, in reality, the aircraft response is only close to ideal.

In the course of the derivation a linear relation between control deflection and generated moment was assumed. Although in practice by approximation this is often correct, the relation can be highly nonlinear for particular aircraft. Nonlinearities can, however, be described as extra parametric uncertainties, against which the PINDI controller is shown to be robust.

In principle every system is linearized to the same low-pass filter when using INDI, with only small errors remaining. To then obtain a

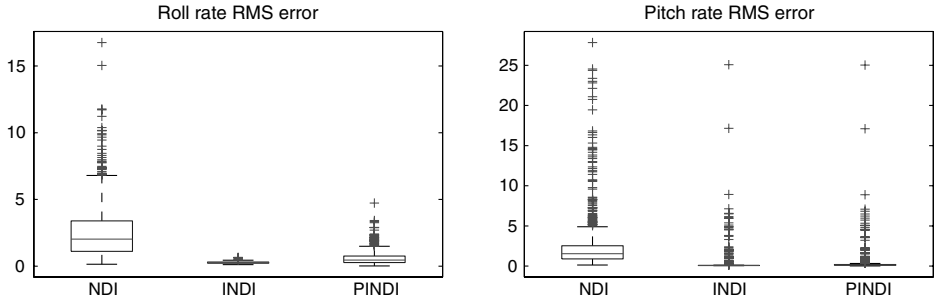

a) Roll rate b) Pitch rate

Fig. 5 Box plots of a Monte Carlo simulation of the inner loop response of the UAV controlled using NDI, INDI, and PINDI, subject to mismatches in the aerodynamic model, both in stability and control derivatives. The NDI and PINDI controllers are subject to sensor measurement time delays, and the INDI controlled system is not.

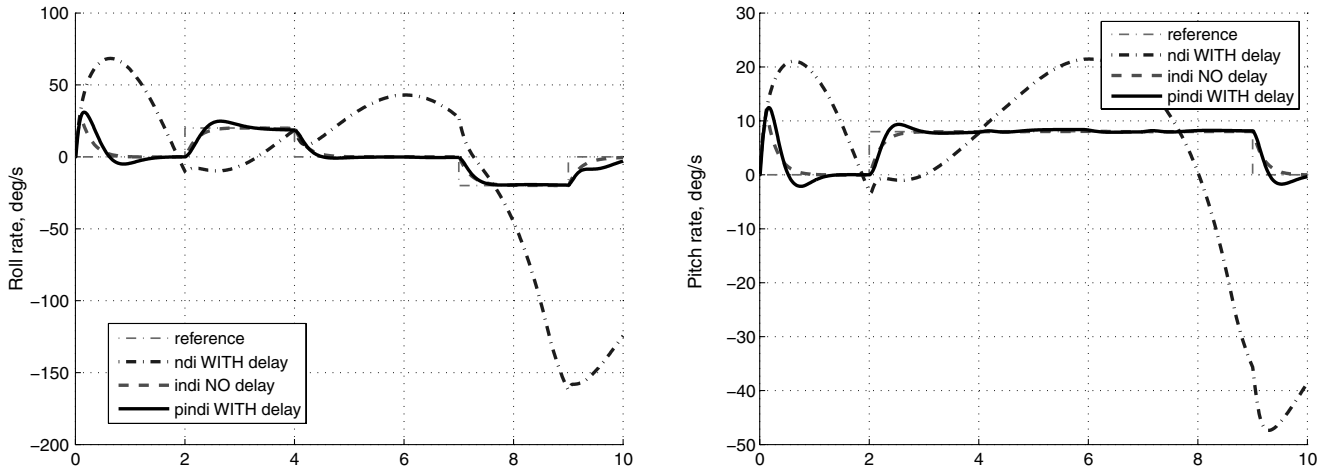

a) Roll rate b) Pitch rate

Fig. 6 The inner loop response of the UAV controlled using NDI, INDI, and PINDI, subject to a mismatch in the center of gravity of 50% mean aerodynamic chord toward the rear and the right of the aircraft. The NDI and PINDI controllers are subject to sensor measurement time delays, and the INDI controlled system is not.

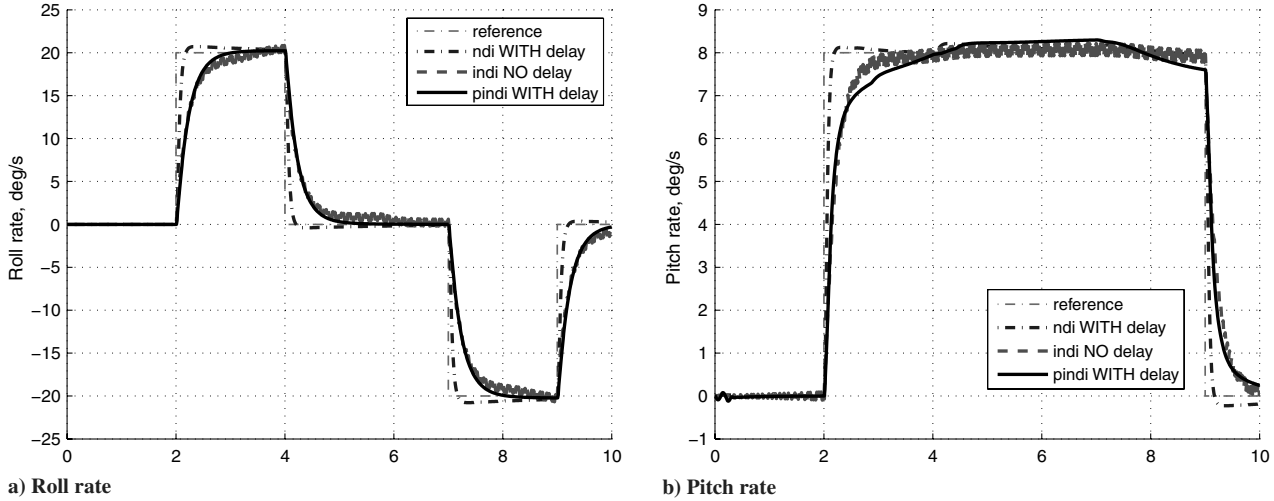

a) Roll rate b) Pitch rate

Fig. 7 The inner loop response of the UAV controlled using NDI, INDI, and PINDI, subject to a mismatch in the moment of inertia of 50%. The NDI and PINDI controllers are subject to sensor measurement time delays, and the INDI controlled system is not.

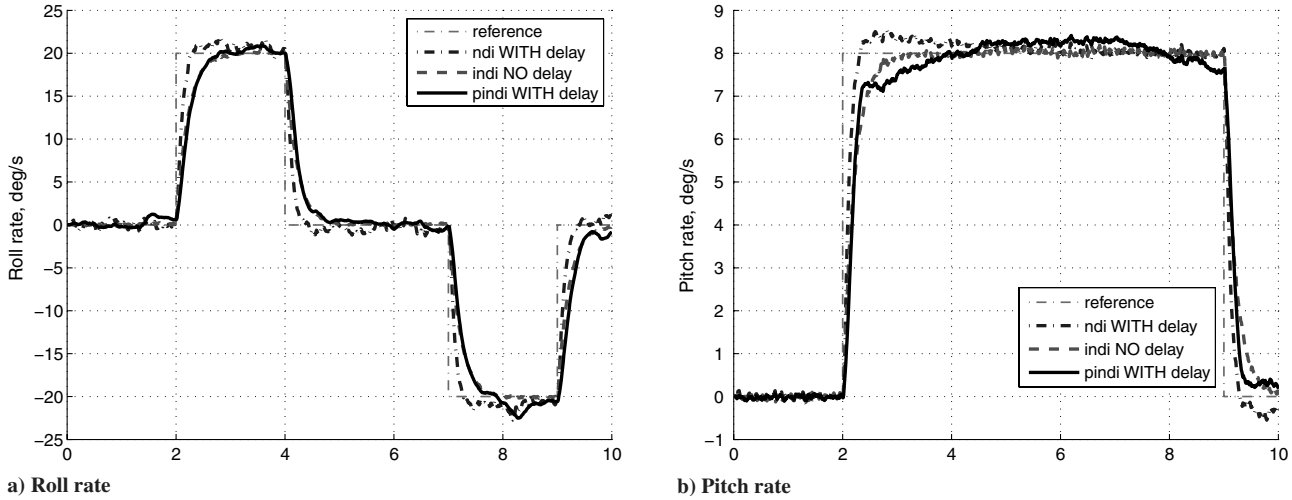

a) Roll rate b) Pitch rate

Fig. 8 The inner loop response of the UAV controlled using NDI, INDI, and PINDI, subject to sensor noise. Noise on angular rates is 0.1°/s, on flow angle measurements it is 0.25°, and on angular acceleration measurements it is 1°/s^2. The NDI and PINDI controllers are subject to sensor measurement time delays, and the INDI controlled system is not.

more accurate filter, only small corrections are required. Hence it should be possible to have an online adaptive algorithm to make these small adjustments to the coefficients, to obtain the ideal response. Using simulated flight data from a well-modeled aircraft controlled using an ideal INDI controller, it is found that coefficients for the predictive filter of Eq. (46) can be computed, such that the PINDI response matches the ideal INDI performance in every aspect.

X. Conclusions

INDI and the practically available PINDI require less aircraft state information, but result in better robust performance than regular NDI. Furthermore INDI and PINDI require significantly less model information in both qualitative and quantitative sense than NDI.

Because angular accelerations are not readily available, and because it is shown that INDI is sensitive to measurement delays a linear predictive filter is designed to predict the angular accelerations from only angular rates and references thereof. It is demonstrated that using PINDI the robust performance improves compared with regular NDI for aerodynamic model, inertia, and CG mismatch.

Because the stability is not endangered for any type of mismatch, it is possible to implement the PINDI control algorithm and fly aircraft with hardly any knowledge of the model.

Acknowledgments

The authors would like to express their gratitude to the Dutch aerospace laboratory Nationaal Lucht- en Ruimtevaartlaboratorium for making this research possible, with special thanks to Jan Breeman, Skander Taamallah, and Henk Jentink, and to Nuno Filipe, Mathilde Ducamp, Wiebe Berkelaar, Armin Oonk, Gijsbert Bakker, and Mark Verveld of Delft University of Technology for their fruitful discussions and suggestions to the subject.

References

[1] Slotine, J., and Li, W., *Applied Nonlinear Control*, Prentice–Hall, Upper Saddle River, NJ, 3rd ed., 1991, pp. 207–271.

[2] Reiner, J., Balas, G. J., and Garrard, W. L., "Flight Control Design Using Robust Dynamic Inversion and Time-Scale Separation," *Automatica*, Vol. 32, No. 11, 1996, pp. 1493–1504. doi:10.1016/S0005-1098(96)00101-X

[3] Juliana, S., Chu, Q. P., Mulder, J. A., and van Baten, T. J., "The Analytical Derivation of Non-linear Dynamic Inversion Control for Parametric Uncertain System," *AIAA Guidance, Navigation, and Control Conference and Exhibit*, AIAA, Reston, VA, 2005.

[4] Lee, H. P., Reiman, S. E., Dillon, C. H., and Youssef, H. M., "Robust Nonlinear Dynamic Inversion Control for a Hypersonic Cruise Vehicle," *AIAA Guidance, Navigation and Control Conference and*

Exhibit, AIAA, Reston, VA, 2007.

[5] Smith, P. R., "A Simplified Approach to Nonlinear Dynamic Inversion Based Flight Control," *AIAA Atmospheric Flight Mechanics Conference and Exhibit*, AIAA, Reston, VA, 1998.

[6] Bacon, B. J., and Ostroff, A. J., "Reconfigurable Flight Control Using Nonlinear Dynamic Inversion with a Spacial Accelerometer Implementation," *AIAA Guidance, Navigation, and Control Conference and Exhibit*, AIAA, Reston, VA, 2000.

[7] Williams, J. E., and Vukelich, S. R., *The USAF Stability and Control Digital DATCOM*, U.S. Air Force Flight Dynamics Lab., Dayton, OH, 1979.

[8] Drela, M., and Youngren, H., *AVL 3.26 User Primer*, MIT Aero/Astro, Aerocraft, Inc., Cambridge, MA, 2006.

[9] da Costa, R. R., Chu, Q. P., and Mulder, J. A., "Reentry Flight Controller Design Using Nonlinear Dynamic Inversion," *Journal of Spacecraft and Rockets*, Vol. 40, No. 1, 2003, 64–71.

[10] Gao, X. Z., and Ovaska, S. J., "Acceleration Signal Estimation Using Neural Networks," *Measurement Science and Technology*, Vol. 12, No. 102001.

[11] Väliviita, S., and Ovaska, S. J., "Delayless Recursive Differentiator with Efficient Noise Attenuation for Control Instrumentation," *Signal Processing*, Vol. 69, No. 3, 1998, pp. 267–280.

[12] Gianfelici, F., "A Novel Technique for Indirect Angular Acceleration Measurement," *IEEE International Conference on Computational Intelligence for Measurement Systems and Applications*, IEEE Publications, Piscataway, NJ, 2005.

[13] Garret, A., Aguilar, M., and Barniv, Y., "A Recurrent Neural Network Approach to Virtual Environment Latency Reduction," *International Joint Conference on Neural Networks*, IEEE Publications, Piscataway, NJ, 2002.

[14] Burden, R. L., and Faires, J. D., *Numerical Analysis*, 7th ed., Brooks/Cole, Pacific Grove, CA, 2001, p. 171.

[15] Huisman, H., "Fault Tolerant Flight Control based on Real-Time Physical Model Identification and Nonlinear Dynamic Inversion," Master's Thesis, Delft Univ. of Technology, 2007.